International Journal of Thermofluid Science and Technology (2021)
Volume 8, Issue 1, Paper No. 080101
https://doi.org/10.36963/IJTST.2021080101
Research Article

Investigation of the convective heat transfer and friction factor of magnetic Ni nanofluids within cylindrical pipes

Mahammedi Abdelkader [1,2], Houari Ameur [3,*], Younes Menni [4]

[1]*Department of Technology, Ziane Achour University of Djelfa, Algeria.*
[2]*Mechanical Engineering Research Laboratory (LaRTFM), ENPO of Oran, Algeria.*
[3]*Department of Technology, University Centre of Naama, P.O. Box 66, Naama 45000, Algeria.*
[4]*Department of Physics, Faculty of Sciences, Abou Bekr Belkaid University, P.O. Box 119, 13000, Tlemcen, Algeria.*

Received: 12 September 2020; Received in revised form: 22 November 2020; Accepted: 21 December 2020; Published online 18 January 2021

Abstract

The current paper reports the results of numerical research on the magnetic Ni nanofluid flowing in a tube, developing turbulent flows under constant heat flux conditions. The numerical investigations are conducted for a Reynolds number range from 3,000 to 22,000, and a particle concentration range of 0% to 0.6%. The effects of the Reynolds number on the friction factor and Nusselt number are computed and compared satisfactorily with the experimental results of the literature. The classical correlations of Gnielinski, Notter – Rouse, and Pak and Cho are verified by predicting the Nusselt number of the Ni nanofluid. The obtained results revealed an enhancement in the heat transfer with the increase of magnetic Ni particle volume fraction and Reynolds number.

Keywords: Ni-nanofluid; Heat transfer; CFD; Nusselt number; Friction factor.

1. Introduction

The expression nanofluid was once utilized for the earliest time by Choi [1]. After that, several researchers persevered in his work and concentrated on modeling nanofluids thermal conductivity, these days the emphasis is on the performance of nanofluid fluid flow and heat transfer [2-4].

Research has shown in general that improving the thermal conductivity depends much more on nanoparticles than on the base fluid; thus, researchers have concentrated their efforts on analyzing a large diversity of nanoparticles [5, 6]. Sekrani et al. [7] conducted a new work on estimating the heat transfer coefficient for Al_2O_3-water in the forced convective turbulent regime, and used comprehensive evaluations of the turbulence models to determine the nanofluid performance assessment.

*Corresponding e-mail: houari_ameur@yahoo.fr; ameur@cuniv-naama.dz (Houari Ameur)

Saha et al. [8] look into the entropy generation and heat transfer behavior of the transitional flow of TiO_2-H_2O nanofluid in a pipe. Their results pointed out that the small size of nanoparticles has the best rate of heat transfer for x = 6% and, the TiO_2-H_2O nanofluid displays an elevated rate of heat transfer with a multi-phase model relative to a single-phase model. No most advantageous number of Reynolds was found, which could reduce the generation of the total entropy. A new correlation is suggested to measure the Nusselt number with a standard error deviation of less than 0.5%.

Senthilraja et al. [9] investigated experimentally the thermal conductivity of Al_2O_3-H_2O, CuO-H_2O, and Al_2O_3–CuO/H_2O. The two-step approach was followed to get the hybrid nanofluid. Three specific volume fractions of nanofluids (0.05, 0.1, and 0.2%) have been prepared by dispersing in water the Al_2O_3 and CuO nanoparticles. Hybrid and single nanofluid properties were measured at different temperatures from 20 to 60 ℃. Received consequences exhibited that the thermal conductivity of nanofluids is the characteristic of temperature and volume fraction. Additionally, the experimental consequences confirmed that a maximum of 9.8% improvement of thermal conductivity was practical at 0.2% particle volume fraction. The theoretical values were evaluated using the measurements of the experimental thermal conductivity values.

Behzadmehr et al. [10] explored numerically the turbulent heat flow in a circular tube with water and 1% Cu. To explore such a flow field, a two-phase mixture model has been applied for the first time. A single-phase model, commonly used in the past for nanofluid heat transfer, is often used to add 1% of Cu nanoparticles, raising the level of Nusselt by more than 15%, without having any noticeable impact on skin friction.

He et al. [11] conducted a numerical analysis was by using both the combined Euler and Lagrange method and the single-phase method for the convective heat transfer of TiO_2 nanofluids in the tube with different aggregate sizes of nanoparticles. Their results displayed an extensive augmentation in the heat transfer of nanofluids, especially in the entry area. Esfe et al. [12] examined experimentally the thermo-physical properties and convective heat transfer performance of MgO-H_2O nanofluid, where the concentration of nanoparticles is less than 1% in the base fluid. They used natural water and nanofluid with particle volume concentration of 0.0625%, 0.125%, 0.25%, 0.5% and 1%. They detected that the most typical models struggle to expect correctly the dynamic viscosity and thermal conductivity of the MgO-H_2O nanofluid. The effects suggested that injecting a low value of nanoparticles, into the base fluid considerably excites the heat transfer to growth. Their tests illustrated that the nanofluid pressure drop is barely upper than that of the base fluid even when the nanoparticles volume concentration increase.

Bozorgan et al. [13] investigated numerically the use of CuO-H_2O nanofluid with a dimension of 20 nm and up to 2% volume fractions of nanoparticles in a radiator of Chevrolet diesel engine. Their results revealed that the heat transfer coefficient and pumping power for CuO-H_2O nanofluid at 2% volume fraction flowing through the flat tubes while the car speed equal 70 km/h and Re = 6000, is respectively 10% and 23.8% higher than that of the base fluid for the specified conditions.

Shah et al. [14] designed an experimental setup using a spiral heat exchanger with water-based SiO_2 nanofluid as coolant with a nanoparticle size equal to 15 nm at varying mass flow rates and air velocity of the fluid to examine its effect on the heat transfer coefficient. From the experimental information, the outlet temperature of the fluid is minimum and the heat transfer is maximum at 0.4% volume concentration. The rise in heat transfer was identified from 160% to 400% than by the use of usual water. They suggested a correlation for different cases among numbers of Reynolds, Prandtl, and Nusselt.

Naraki et al. [15] demonstrated experimentally the impact of CuO-water nanofluids on a vehicle engine's cooling system under the laminar flow. Two methods were employed to get

more stabilized nano-fluids, i.e., modification of pH and addition of the appropriate surfactant. In comparison with the base fluid, they found that the overall heat transfer coefficient was increased by 8% for the volume concentration of 0.4%. Sundar et al. [16] estimated the heat transfer coefficient and the friction factor for different concentrations of magnetic Ni nanofluid flowing in a tube under turbulent flow conditions. Friction factor and Nusselt number correlations were developed on the basis of experimental results.

The aim of this work is to contribute more to the turbulent forced convection of nanofluids in tubes. The "single-phase fluid" approach is used to study the thermal performances of Ni-nanofluids, with the same thermophysical properties found by Sundar et al. [16], i.e., with a particle diameter of 72 nm and low volume fraction (vol.% $\leq$ 0.6). The finite volume method is used to solve the problem. The results acquired by the model are achieved in terms of friction, and Nusselt number, in addition to the comparison with the theoretical and experimental data provided in the literature.

The objective of the present paper is to estimate numerically the heat transfer performance of Ni–water nanofluid under turbulent flow conditions, which has not been studied previously. For this reason, applying the CFD modeling and validate with existing experimental results and correlations could be considered as a practical effort to address this issue.

2. Geometrical configuration

Fig. 1 shows the geometrical configuration of the problem under investigation. It consists of a two-dimensional pipe with length (L) of 1.5 m and a diameter (D) of 0.014 m. The present work investigates the turbulent flows and the corresponding convective heat transfers of water-based/Ni nanofluids under steady-state conditions.

The convective heat transfer coefficient generally augments with the raise of particle concentration or the flow rate. The point of calculating the heat transfer coefficient at this flux is to validate the work with experiment data by using the similar parameters.

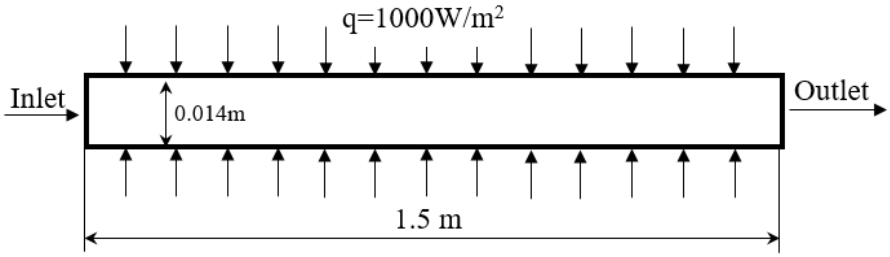

Fig. 1. Numerical domain of the physical problem.

3. Mathematical model

The working nanofluid is modeled as a single-phase fluid with rather different physical properties such as: density, thermal conductivity, and viscosity. The fluid phase was assumed to be continuous. The fluid is Newtonian and incompressible. Flux and heat transfer are considered by continuity, momentum and energy equations. The steady-state governing equations are given, respectively, as follows:

Continuity equation:

$$\nabla\left(\rho_{nf} V_m\right) = 0 \tag{1}$$

Momentum equation:

$$\nabla\left(\rho_{nf} V_m V_m\right) = -\nabla P + \nabla\left(\mu_{nf} \nabla V_m\right) \tag{2}$$

Energy equation:

$$\nabla\left(\rho\vec{v}C_p T_{nf}\right)=\nabla\left(k\nabla T_{nf}\right) \tag{3}$$

Realizable $k-\varepsilon$ turbulent model is used to simulate the turbulence in ANSYS FLUENT proposed by Shih et al. [17], to renormalize the Navier-Stokes and the generation of turbulence kinetic energy due to the velocity gradients.

4. Thermal and physical properties of nanofluids

The thermophysical properties of Ni nanofluid are summarized in Table 1, where the experimental data of Sundar et al. [16] for the absolute viscosity and thermal conductivity data for the Ni nanofluid are used. The density and specific heat of Ni nanofluid are expected for T = 20 ℃ from:

$$\rho_{nf}=\left(1-\varphi\right)\rho_{bf}+\varphi\times\rho_p \tag{4}$$

The specific heat capacity of the nanofluid as a function of the particle volume concentration and individual properties can be computed using the equation given by Pak and Cho [17]. Further details on the density of nanofluids may be found in Ref. [18].

$$C_{p_{nf}}=\left(1-\varphi\right)C_{p_{bf}}+\varphi\times C_{p_p} \tag{5}$$

Table 1: Thermophysical properties of Ni nanofluid

Property	Volume concentration (%)				
	0.0	0.02	0.1	0.3	0.6
ρ (kg/m^3)	998.5	1000.08	1006.40	1022.21	1045.92
k (W/m·K)	0.602	0.6152	0.6579	0.6842	0.7126
μ (mPa·s)	0.79	0.81	0.84	0.97	1.1
Cp (J/kg·K)	4182	4181.25	4178.25	4170.77	4195.54

5. Numerical method and validation

The computational fluid dynamic is used to solve the problem. The governing Eqs. (1), (2), and (3) are solved by the control volume technique. This method is based on the spatial integration of the conservation equations over finite control volumes, converting the governing equations to a set of algebraic equations. The algebraic ‘‘discretized equations”, resulting from this spatial integration process, are sequentially solved throughout the physical domain considered. For the convective and diffusive terms, the second-order upwind method was used while the SIMPLE procedure was introduced for solving iteratively the velocity–pressure coupling algebraic equations.

The heat transfer rate can be determined from Newton’s law of cooling by using a suitable temperature difference ΔT [18]. The convection heat transfer at the pipe wall:

$$q_w^{"}=h\left(T_w-T_m\right) \tag{6}$$

The above equation can be written as:

$$h=\frac{q_w^{"}}{\left(T_w-T_m\right)} \tag{7}$$

where, T_w is the pipe wall temperature at a given location along with the pipe, and T_m is the mean temperature in the pipe at that location where T_w is defined.

$$T_m = \frac{\int_0^R uT\,2\pi r dr}{\int_0^R u\,2\pi r dr} = \frac{\int_0^R uT\,dr}{\int_0^R u\,dr} \tag{8}$$

Nusselt number:

$$Nu = \frac{h L_c}{k} = \frac{q_w^{"} \times (2R)}{(T_w - T_m)} \tag{9}$$

where L_c is the characteristic length.

A common form of Nusselt number:

$$Nu = C\,Re_L^m\,Pr^n \tag{10}$$

where m and n are constant exponents (usually between 0 and 1), and the value of the constant C depends on geometry and flow.

The values of the Nusselt number and friction factor that are acquired by the numerical simulations are validated with the equations and experimental work performed by Sundar et al. [16]. Another validation is made against different well-known correlations, widely used in literature, especially those of Pak and Cho, Notter-Rouse, and Gnielinski.
Gnielinski correlation is given as [19]:

$$Nu = \frac{\frac{f}{8}(Re - 1000)\,Pr}{1 + 12.7\sqrt{\frac{f}{8}}\left(Pr^{2/3} - 1\right)} \quad ; \text{for} \quad 3000 \le Re \le 5\times 10^6 \tag{11}$$

where f is defined as:

$$f = \frac{1}{\left(1.82\ln(Re) - 1.64\right)^2} \quad ; \quad \text{for} \quad 0.5 \le Pr \le 200 \tag{12}$$

Pak and Cho correlation for Al_2O_3 nanofluid [20]:

$$Nu = 0.021\,Re^{0.8}\,Pr^{0.5} \tag{13}$$

for $10^4 < Re < 10^5$; $6.54 < Pr < 12.33$; $0 < \varphi < 0.3$

Notter-Rouse equation [21]:

$$Nu = 5 + 0.015\,Re^{0.856}\,Pr^{0.347} \tag{14}$$

The correlation of Sundar et al. [16] for Ni-nanofluid:

$$Nu_{\mathrm{Re}g} = 0.0221\,Re^{0.8}\,Pr^{0.5}\,(1+\varphi)^{0.54} \tag{15}$$

for: $3000 < Re < 22,000$; $3.72 < Pr < 6.37$; $0 < \varphi < 0.6\%$

The friction factor correlation of Sundar et al. [16] for Ni-nanofluid:

$$f_{\mathrm{Re}g} = 0.35662\,Re^{-0.25}\,(1+\varphi)^{0.2375} \tag{16}$$

for: $3000 < Re < 22,000$; $3.72 < Pr < 6.37$; $0 < \varphi < 0.6\%$.

6. Boundary conditions

The nanofluid is composed of particles of Ni and water, the fluid enters with a uniform temperature T = 293 K and at a fixed Re number. Hence, the inlet velocity (V_i) varies according to the concentration of the nanoparticles. No-slip conditions and a uniform heat flux q = 1000 W/m^2 are applied at the wall.

7. Mesh tests

The discretization grid is uniform, and it is refined near the tube wall, where the temperature gradient is significant. We need to vary the mesh to get the accepted level of the tolerance, which can be found out from the grid independence test.

This is done by varying the mesh size from coarse to fine, and checking the output result for each mesh. The results of the different mesh test are provided in Fig. 2. The best trend between the reliability and the reduced computational time allowed us to select the grid with 183,060 nodes as the most efficient.

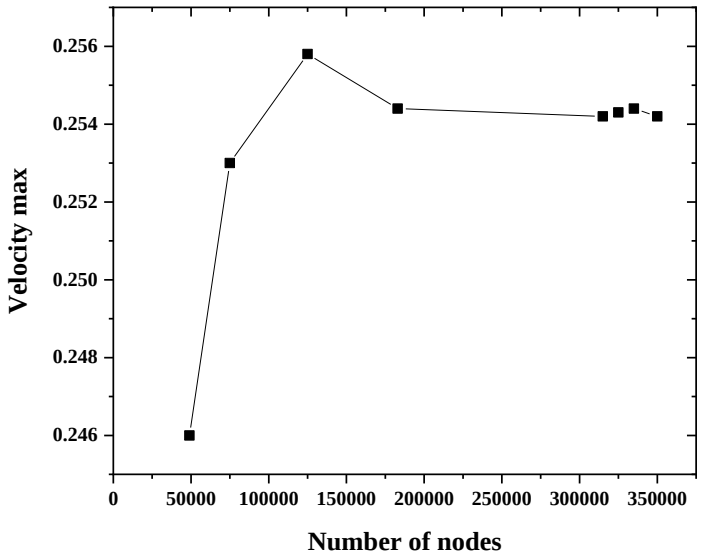

Fig. 2. Grid dependency test

8. Results and discussion

The CFD method has proved its efficiency in the investigation of many industrial problems [22-27]. In our paper, the solver was first validated against the experimental data of Sundar and Singh [12]. The results were achieved by using the single-phase model for *Re* from 30 $\times 10^2$ to 22 $\times 10^4$ and φ and φ in the range of 0 - 6%. In all cases, the size of the spherical particles was considered equal to 72 nm.

8.1. Temperature distributions of nanofluids

Fig. 3 provides the temperature plots in the centerline tube for Reynolds number of 5,000 and 15,000. The nanofluid is heated from the tube wall and the temperature becomes high along with the tube. The temperature raises with the axial position under the heating condition. The temperature of nanofluid is much higher at Reynolds number of 5,000 than that at *Re* = 15,000, due to the intensified heat transfer coefficient at high *Re*.

Fig. 4 shows the variation of the heat transfer coefficient for different volume concentrations of Ni nanofluid estimated by Eq. (9). It is evident that the nanofluids yield an increase in the heat transfer coefficients with the rise of concentration.

Fig. 5 provides further comparisons in terms of the average heat transfer coefficient h for one of the three cases $\varphi = 0.02$. These results are obtained by using the single-phase model, which shows an acceptable agreement with the experimental data.

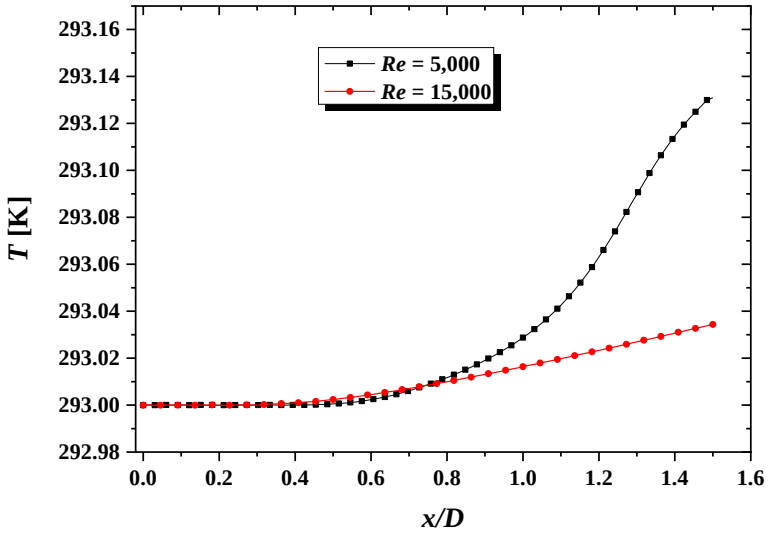

Fig. 3. Axial profiles of the convective heat transfer coefficient.

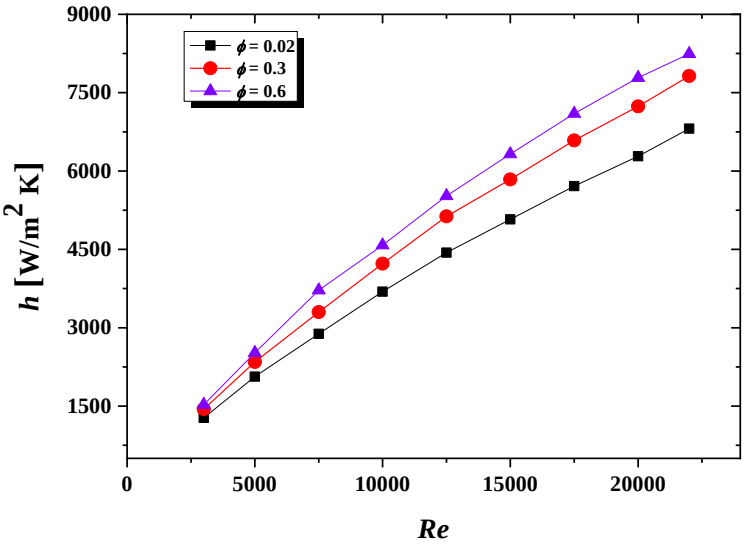

Fig. 4. Heat transfer coefficient of Ni nanofluid as a function of particle concentration and Reynolds number.

8.2.Nusselt number

The predicted Nusselt number of water is presented in Fig. 6 against the experimental data of Sundar et al. [16] and the correlation of Gnielinski (Eq. 11). The deviation in *Nu* values between the correlation of Sundar and our simulation is around ± 0.8%.

For Fig. 7, the nanofluid volume fraction of 0.02 was used. We notice that the numerical simulation is identical to that of Sundar equation and closer to the experimental result better than the results of the rouse and Gnielinski correlations.

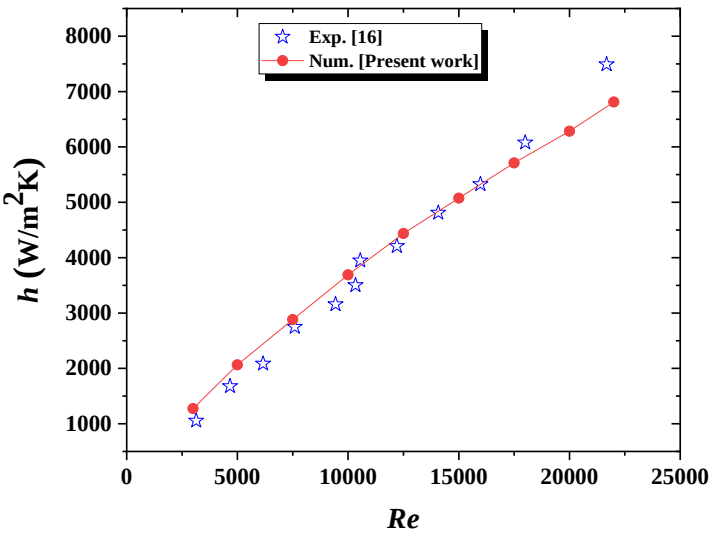

Fig. 5. Validation of the heat transfer coefficient for φ = 0.02 with the experimental data.

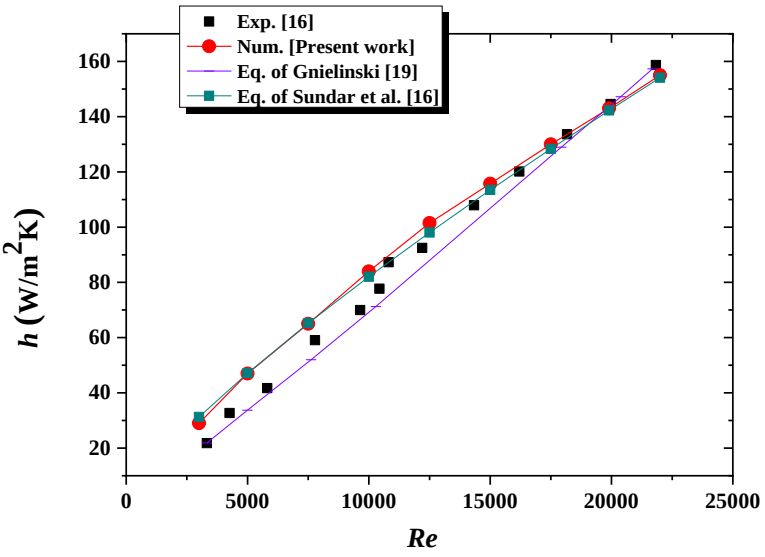

Fig. 6. Nusselt number of water vs. Reynolds number (validation).

For Fig. 8, the nanofluid volume fraction of 0.02 was employed. We observe a combination of numerical simulation and Sundar's correlation and experimentation for *Re* less than 1,250. The numerical simulation is closer to the experimental data better than those with the proposed literature correlations.

For φ = 0.3 and φ = 0.6 (Figs. 9 and 10, respectively), an excellent agreement between our predicted results and the experimental data of Sundar et al. [16] until *Re* = 10,000, while the discrepancy increases between these results for *Re* higher than 10,000. However, the correlation of Sundar and his co-workers seems to provide almost similar results as our predictions for *Re* > 10,000.

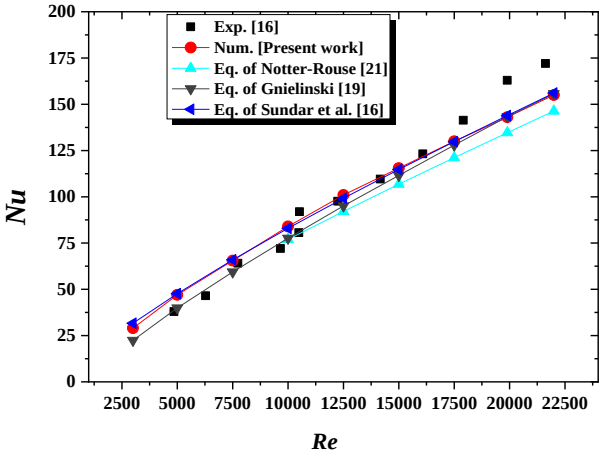

Fig. 7. Variations of the Nusselt number as a function of the Reynolds number for φ = 0.02. Comparison between the numerical results of Ni nanofluid and the proposed correlations

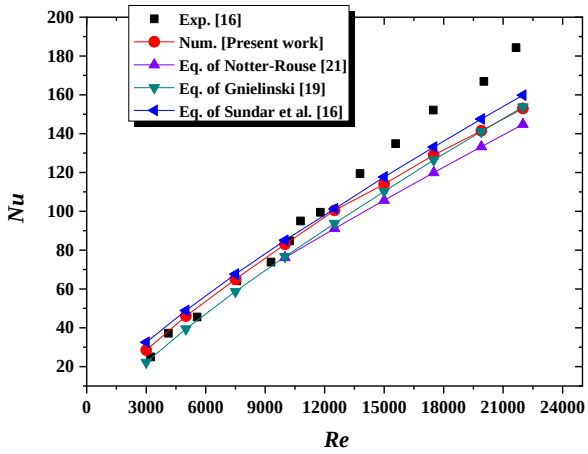

Fig. 8. Variations of the Nusselt number as a function of the Reynolds number for φ = 0.1. Comparison between the numerical results of Ni nanofluid and the proposed correlations.

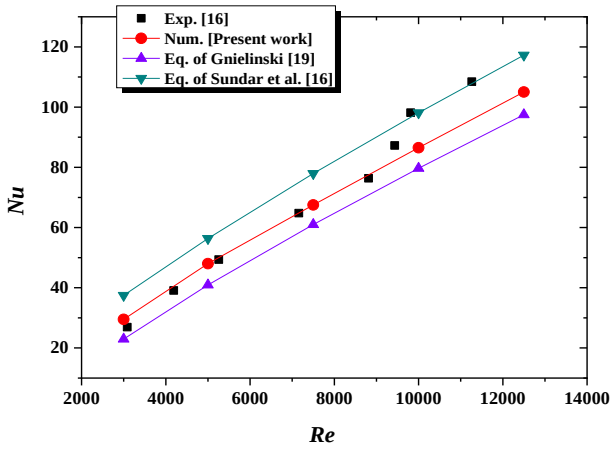

Fig. 9: Variations of the Nusselt number as a function of the Reynolds number for φ = 0.3. Comparison between the numerical results of Ni nanofluid and the proposed correlations.

8.3.Friction factor

Fig. 11 presents the friction coefficient vs. *Re* for several volume fractions (φ = 0.1, 0.3, and 0.6%). As observed in this figure, the friction coefficient decreases with the increase in *Re* for different volume fractions of Ni nanofluid. It is also noted that our numerical results are closer to the experimental result of Sundar et al. [16] than those to the equation of these authors with an average deviation of 3.12%.

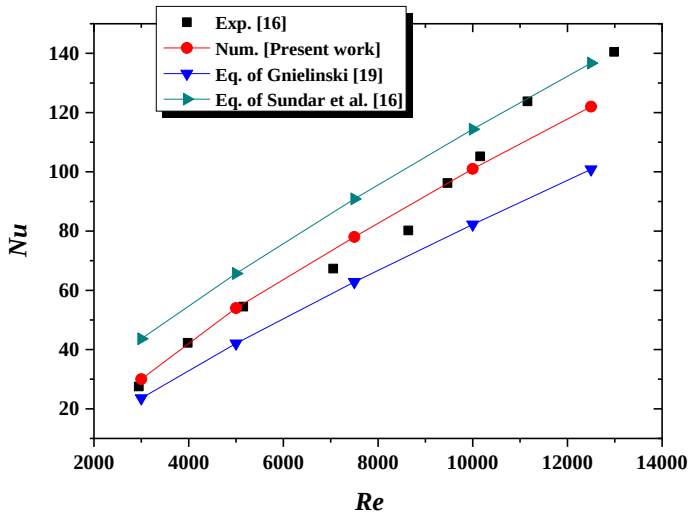

Fig. 10: Variations of the Nusselt number as a function of the Reynolds number for φ = 0.6. Comparison between the numerical results of Ni nanofluid and the proposed correlations.

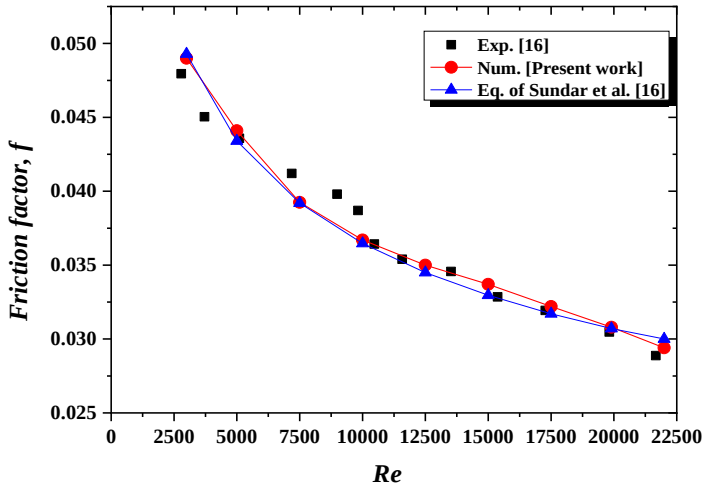

(a)

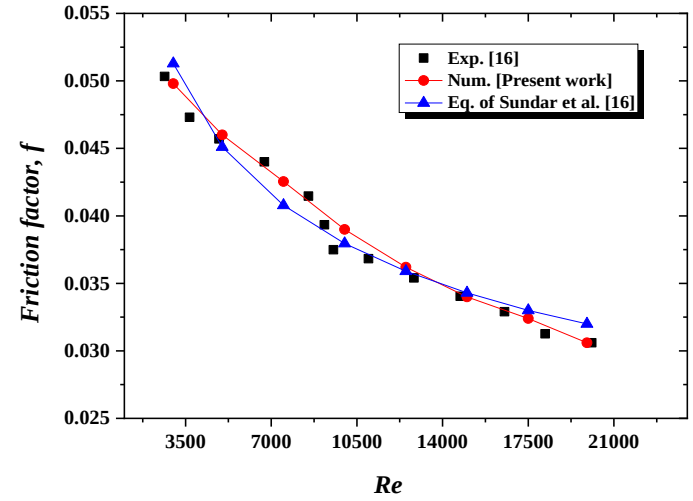

(b)

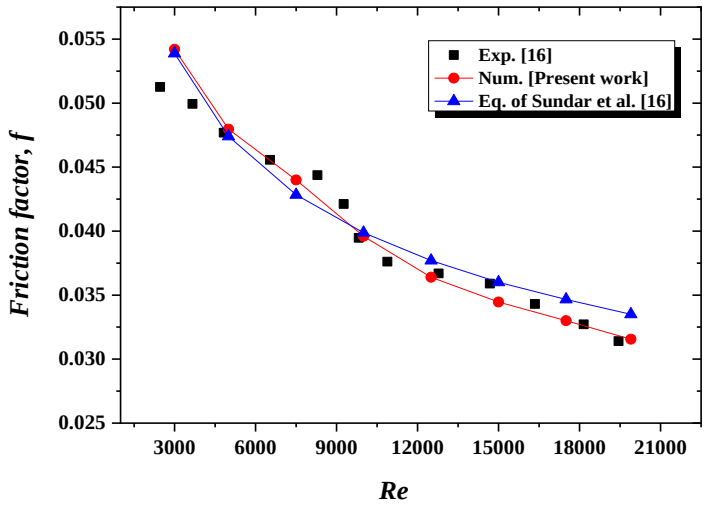

(c)

Fig. 11. Variations of the friction factor as a function of the Reynolds number. Comparison between the present simulations and the experimental and equation developed by Sundar et al. (a) φ = 0.1%, (b) φ = 0.3%, (c) φ = 0.6%.

8.4. Roughness effect

Fig. 12 shows the Darcy friction factor of the fluids with two different roughness heights K_s/D = 0.0267 and 0.0357 at different Reynolds numbers. The friction factor raises with the raise of the roughness height, but it decreases with the increase of Reynolds number. As a consequence, the increase of the roughness height augments the pressure drop resulting in an elevated price in practical applications. In the above sections, we note that the ratio K_s/D was set to 0.

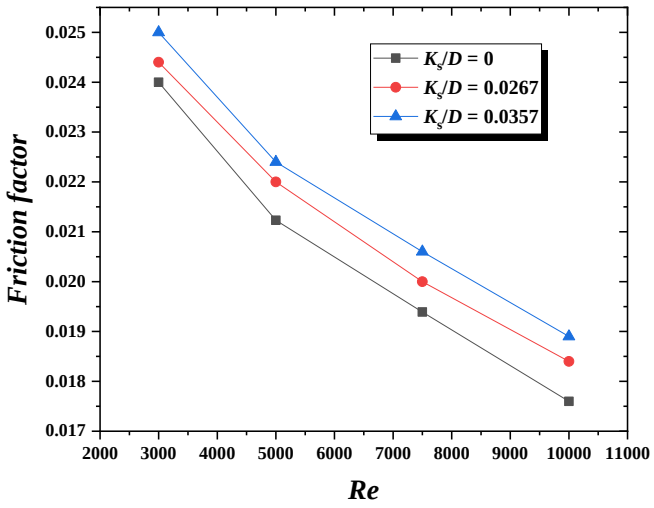

Fig. 12. Variations of the friction factor ratios vs. Reynolds number and the roughness height (K_s)

9. Conclusion

The hydrodynamic and thermal behaviors of water–Ni nanofluids flowing through a uniformly heated tube in stationary conditions were inspected. The study was achieved under turbulent flow conditions for a wide range of Reynolds number. Various volume fractions were also employed to perform the investigations. The predicted results were evaluated against several experimental data and correlations that are available in the literature, where a satisfactory agreement was found.

The obtained results revealed an enhancement in the heat transfer by using Ni nanofluids with respect to the base fluid. The enhancement has been more increased with the rise of the particle volume fraction, with relatively high thermal conductivity. The enhancement in the heat transfer rates of Ni nanofluid is due to the influence of particle Brownian motion and micro-convection of the particles in the base fluid. Compared to the base fluid, an increase in the absolute viscosity of Ni nanofluid is reached with increasing particle concentration, while a decrease is obtained with the temperature.

In addition, an increase in the friction factor (f) has been observed with increasing roughness height, while it decreases with the rise of Reynolds number. Consequently, the increased roughness height may yield an elevated price in practical applications due to the significant pressure drop.

References

[1] S. Choi, Enhancing thermal conductivity of fluids with nanoparticles, in: D. A. Siginer, H. P. Wang, (Eds.), Developments and Applications of Non-Newtonian Flows, ASME, New York, FED-Vol. 231/MD-Vol. 66, 1995, pp. 99-105.

[2] F.A. Abbassi, M. Nazari, M.M. Shahmardan, Numerical study of heat transfer and flow bifurcation of CuO nanofluid in sudden expansion microchannel using two-phase model, Modern Mechanical Engineering 7 (2017) 57-72.

[3] M. Nayak, HHR impact on 3D radiative stretched flow of Cu-H2O nanofluid influenced by variable magnetic field and convective boundary condition, International Journal of Thermofluid Science and Technology 6 (2019) 19060202.

[4] Y. Menni, A.J. Chamkha, G. Lorenzini, N. Kaid, H. Ameur, M. Bensafi, Advances of nanofluids in solar collectors—a review of numerical studies advances of nanofluids in solar collectors—a review of numerical studies, Math Model Eng Probl 6 (2019) 415-427.

[5] M. Uddin, A.F. Hoque, M. Rahman, K. Vajravelu, Numerical simulation of convective heat transport within the nanofluid filled vertical tube of plain and uneven side walls, International Journal of Thermofluid Science and Technology 6 (2019) 19060101.

[6] Y. Menni, A.J. Chamkha, N. Massarotti, H. Ameur, N. Kaid, M. Bensafi, Hydrodynamic and thermal analysis of water, ethylene glycol and water-ethylene glycol as base fluids dispersed by aluminum oxide nano-sized solid particles, International Journal of Numerical Methods for Heat & Fluid Flow (2020).

[7] G. Sekrani, S. Poncet, P. Proulx, Modeling of convective turbulent heat transfer of water-based Al_2O_3 nanofluids in an uniformly heated pipe, Chemical engineering science 176 (2018) 205-219.

[8] G. Saha, M.C. Paul, Analysis of heat transfer and entropy generation of TiO2-water nanofluid flow in a pipe under transition, Procedia Engineering 105 (2015) 381-387.

[9] S. Senthilraja, K. Vijayakumar, R. Gangadevi, A comparative study on thermal conductivity of Al_2O_3/water, CuO/water and Al2O3–CuO/water nanofluids, Digest Journal of Nanomaterials and Biostructures 10 (2015) 1449-1458.

[10] A. Behzadmehr, M. Saffar-Avval, N. Galanis, Prediction of turbulent forced convection of a nanofluid in a tube with uniform heat flux using a two phase approach, International Journal of Heat and Fluid Flow 28 (2007) 211-219.

[11] Y. He, Y. Men, Y. Zhao, H. Lu, Y. Ding, Numerical investigation into the convective heat transfer of TiO_2 nanofluids flowing through a straight tube under the laminar flow conditions, Applied thermal engineering 29 (2009) 1965-1972.

[12] M.H. Esfe, S. Saedodin, M. Mahmoodi, Experimental studies on the convective heat transfer performance and thermophysical properties of MgO–water nanofluid under turbulent flow, Experimental thermal and fluid science 52 (2014) 68-78.

[13] N. Bozorgan, K. Krishnakumar, N. Bozorgan, Numerical study on application of cuo-water nanofluid in automotive diesel engine radiator, (2012).

[14] S. Shah, K.K. Kumar, Experimental Study & Heat Transfer Analysis on Copper Spiral Heat Exchanger Using Water Based SiO_2 Nanofluid as Coolant, World Journal of Nano Science and Engineering 8 (2018) 57.

[15] M. Naraki, S. Peyghambarzadeh, S. Hashemabadi, Y. Vermahmoudi, Parametric study of overall heat transfer coefficient of CuO/water nanofluids in a car radiator, International Journal of Thermal Sciences 66 (2013) 82-90.

[16] L.S. Sundar, M.K. Singh, I. Bidkin, A.C. Sousa, Experimental investigations in heat transfer and friction factor of magnetic Ni nanofluid flowing in a tube, International Journal of Heat and Mass Transfer 70 (2014) 224-234.

[17] T.-H. Shih, W.W. Liou, A. Shabbir, Z. Yang, J. Zhu, A new k-epsilon eddy viscosity model for high Reynolds number turbulent flows: Model development and validation, (1994).

[18] Y. Cengel, Heat and mass transfer: fundamentals and applications (McGraw-Hill Higher Education, 2014).

[19] V. Gnielinski, New equations for heat and mass transfer in turbulent pipe and channel flow, Int. Chem. Eng. 16 (1976) 359-368.

[20] B.C. Pak, Y.I. Cho, Hydrodynamic and heat transfer study of dispersed fluids with submicron metallic oxide particles, Experimental Heat Transfer an International Journal 11 (1998) 151-170.

[21] R. Notter, C. Sleicher, A solution to the turbulent Graetz problem—III Fully developed and entry region heat transfer rates, Chemical Engineering Science 27 (1972) 2073-2093.

[22] H. Ameur, Pressure drop and vortex size of power law fluids flow in branching channels with sudden expansion, Journal of Applied Fluid Mechanics 11 (2018) 1739-1749.

[23] H. Ameur, Investigation of the performance of V-cut turbines for stirring shear-thinning fluids in a cylindrical vessel, Periodica Polytechnica Mechanical Engineering 64 (2020) 207-211.

[24] H. Ameur, 3D hydrodynamics involving multiple eccentric impellers in unbaffled cylindrical tank, Chinese Journal of Chemical Engineering 24 (2016) 572-580.

[25] H. Ameur, Effect of the shaft eccentricity and rotational direction on the mixing characteristics in cylindrical tank reactors, Chinese Journal of Chemical Engineering, 24 (2016) 1647-1654.

[26] H. Ameur, Mixing of shear thinning fluids in cylindrical tanks: effect of the impeller blade design and operating conditions. International Journal of Chemical Reactor Engineering 14(2016) 1025-1034.

[27] H. Ameur, Energy efficiency of different impellers in stirred tank reactors, Energy 93 (2015) 1980-1988.